

Impact of Climate and Land Use/Cover Changes on Streamflow in Yadot Watershed, Genale Dawa Basin, Ethiopia

Authors: Mustefa Abdule, Abay, Muluneh, Alemayehu, and Woldemichael, Abraham

Source: Air, Soil and Water Research, 16(1)

Published By: SAGE Publishing

URL: <https://doi.org/10.1177/11786221231200106>

BioOne Complete (complete.BioOne.org) is a full-text database of 200 subscribed and open-access titles in the biological, ecological, and environmental sciences published by nonprofit societies, associations, museums, institutions, and presses.

Your use of this PDF, the BioOne Complete website, and all posted and associated content indicates your acceptance of BioOne's Terms of Use, available at www.bioone.org/terms-of-use.

Usage of BioOne Complete content is strictly limited to personal, educational, and non-commercial use. Commercial inquiries or rights and permissions requests should be directed to the individual publisher as copyright holder.

BioOne sees sustainable scholarly publishing as an inherently collaborative enterprise connecting authors, nonprofit publishers, academic institutions, research libraries, and research funders in the common goal of maximizing access to critical research.

Impact of Climate and Land Use/Cover Changes on Streamflow in Yadot Watershed, Genale Dawa Basin, Ethiopia

Air, Soil and Water Research
Volume 16: 1–15
© The Author(s) 2023
Article reuse guidelines:
sagepub.com/journals-permissions
DOI: 10.1177/11786221231200106



Abay Mustefa Abdule¹, Alemayehu Muluneh²
and Abraham Woldemichael²

¹Agarfa Agricultural TVET College, Ethiopia, and ²Hawassa University, Ethiopia

ABSTRACT: Climate and land use/cover (LULC) changes are essential factors that influence hydrological regimes by altering the groundwater recharge and river flow. This study investigated the separate and combined impact of climate and LULC changes on streamflow. The Soil and Water Assessment Tool (SWAT) was used to simulate streamflow under near-term (2021–2050) and mid-term (2051–2080) period against 1985 to 2015 baseline period. The Cellular Automata (CA)-Markov chain model was used to predict the future LULC change. The three-ensemble average of regional climate models (CCLM4.8, RACMO22T, EC-EARTH) under RCP 4.5 and RCP 8.5 emission scenarios were applied for future climate projection. The LULC predictions between 2035 and 2055 showed an increase in agricultural land, grassland, settlement areas and woodlands by 44.02%, 30.35%, 69.2%, and 55.05%, respectively, while forest and scrub/bush lands showed a decrease by decrease by 21.53% and 11.08%, respectively. The annual, wet, and dry seasons rainfall projections increased by 0.13%, 0.02%, and 0.85% respectively, during the near term period under RCP 4.5 scenarios. Overall, the annual, wet, and dry season rainfall projections showed slightly increasing tendency. The temperature projection consistently indicated a warmer future with the highest mean annual projected temperature being 2.0°C under high emission scenario during the midterm period. The projected streamflow under the combined impact of climate and LULC changes will increase by up to 8.72% in wet seasons and by up to 6.62% in dry seasons during the near-term period under RCP4.5 scenarios. Similarly, the projected mean annual streamflow will increase by up to 8.13%. The annual, wet and dry season's streamflow projections showed a consistent increase during both near and midterm periods under both climate scenarios. Understanding the future response of streamflow under climate and LULC changes is crucial to plan adaptation options for water resources management under *future warming condition*.

KEYWORDS: CA-Markov, climate change impact, LULC change, streamflow, SWAT

RECEIVED: April 24, 2023. **ACCEPTED:** August 21, 2023.

TYPE:Original Article

CORRESPONDING AUTHOR: Alemayehu Muluneh, Department of Biosystems Engineering, Hawassa University, Hawassa 05, Ethiopia. Email: muluneh96@yahoo.com

Introduction

Climate and land use/cover (LULC) changes have significant impacts on the hydrological processes such as precipitation, evaporation, runoff (J. Li et al., 2012, Yin et al., 2017). Many studies reported the extensive impact of climate and LULC changes on streamflow (Abera et al., 2019; Ning et al., 2016).

Changes in climate and LULC are the two inseparable linked global environmental challenges the world faces today (IPCC, in press). Since the beginning of the industrial revolution in the mid-eighteenth century, the contribution of human activity to climate change has increased dramatically, by increasing the atmospheric concentrations of greenhouse gases. The warming temperature trend and the changing rainfall pattern are noticeable features of change in climate that directly impact almost all other hydrological responses (Azari et al., 2016). Therefore, quantifying the impact of climate and LULC changes separately and in combination are essential for planning adaptation options for water resources sustainable development (Yang et al., 2017).

Water resources are currently under severe pressure because of climate change impacts and anthropogenic interventions, which include dynamics of land-use, population and economic growth (IPCC, 2013). Climate change due to human activity has led to changes in rainfall patterns and more frequent heavy

precipitation events, which have been significant effects on the ecological system (Simane et al., 2016) and alters streamflow through changes in temperature, rainfall, and evapotranspiration. Similarly, changes in LULC alters infiltration and evapotranspiration, which results in changes to the volume of runoff (Umair et al., 2019; Zhang et al., 2017). However, the comparative role of climate and LULC changes on streamflow may differ spatially due to the rate and magnitude of climate and LULC changes. Therefore, such studies are critical in planning and management of water resources sustainably.

Past studies on response of streamflow on climate change in Genale Dawa basin reported mixed results. For instance, Gragn et al. (2019) found a significant increase in the mean annual streamflow over the two projected periods (2018–2047 and 2048–2077) compared to the baseline period (1988–2017) under both RCP4.5 and RCP8.5 scenarios. The same study (Ibid) reported the average total flow volume increases in Kiremt season (June– September) and decrease in Bega season (October– January) in the future. In contrast to the above mentioned results, the recent study by Gebrechorkos et al. (2023) reported a decrease in the projected annual streamflow in the 2020s, 2050s, and 2080s under SSP245 and SSP585 scenarios relative to the reference period (1981–2010) in Genale Dawa Basin. Seasonally, there is a decrease in streamflow during Belg



Creative Commons Non Commercial CC BY-NC: This article is distributed under the terms of the Creative Commons Attribution-NonCommercial 4.0 License (<https://creativecommons.org/licenses/by-nc/4.0/>) which permits non-commercial use, reproduction and distribution of the work without further permission provided the original work is attributed as specified on the SAGE and Open Access pages (<https://us.sagepub.com/en-us/nam/open-access-at-sage>).

(March, April and May) season in the 2020s but will increase in the 2050s and 2080s (Gebrechorkos et al., 2023). However, the streamflow will be higher during the summer season (July, August, and September) in all periods. Thus, contradiction on findings in existing literature imply the need for *further research* in this topic.

Recently, various studies investigated the integrated impact of climate and LULC change on hydrologic processes (Aboelnour et al., 2019; Hyandye et al., 2018; Koch et al., 2015). Thus, many studies consistently highlight the streamflow, as the key element of hydrology, likely impacted by projected climatic and LULC changes. For instance, there are studies that reported the more significant impact of climate change on streamflow than LULC change (Aboelnour et al., 2019; Dagnenet Fenta et al., 2018). In *some* research findings, the magnitude of LULC change impact is more than the impacts of climate change (Mwangi et al., 2016; Yin et al., 2017). Thus, site-specific investigation and Quantification of the separate and combined impacts of climate and LULC change is a prerequisite for formulating plans and implementing effective adaptation measures of climate change (Clerici et al., 2019; Trolle et al., 2019; Wang et al., 2018).

The Soil and Water Assessment Tool (SWAT) is commonly used to understand the relationship between climate and LULC change on hydrology (Chang et al., 2015; Natkhin et al., 2015). The SWAT tool is effectively utilized in assessing the effect of climate and LULC changes on hydrology in different basins with variable soil, land use, and management requirements across time (Arnold et al., 2012). This model has produced great accuracy for current and future predictions of mean annual and mean monthly streamflow (Anand et al., 2018; Zuo et al., 2016).

Yadot watershed is under threat because of watershed degradation such as deforestation from growing population and due to increasing demand of water mainly for irrigation and other development activities. The watershed is undergoing climate and LULC changes due to agricultural expansion and unplanned and unrestricted settlement because of rapid population growth, deforestation, improper land use and rapid immigration, which adversely alters the hydrology of the watershed. Thus, this research work assessed climate and LULC changes impact on streamflow of Yadot river watershed for the near-term (2021–2050) and mid-term (2051–2080) periods under medium (RCP4.5) and high (RCP8.5) emissions scenarios using SWAT hydrological model and downscaled climatic data from CORDEX-RCMs output. This study was specifically aimed at (1) to predict the future LULC change (2) to assess the projected climate for the near and mid-term periods, (3) to examine the separate and combined impact of climate and LULC changes. Finally, the findings of this study will help to reduce the risks related with future climate and LULC changes in Yadot watershed and the region.

Materials and Methods

Study area description

The Yadot watershed is located, in the Genale Dawa basin of Ethiopia, between 6° 18'N and 6° 51'N and 39°49'E and 39°58'E (Figure 1). The Yadot River starts in the Bale Mountains at an elevation of 4,373 m above mean sea level (m.a.m.s.l) and descends to an elevation of 946 m.a.m.s.l at the watershed's mouth. The watershed covers 735.6 km² area. The Yadot River is perennial, but the flow reduces during the winter and increased during summer season.

The watershed is characterized by various landforms such as valleys, hills, mountains, ridges, and plateaus, which can impact the flow of water and the distribution of vegetation. Areas with steep slopes and high elevations, such as mountains and ridges are typically the source of the river and its tributaries whereas areas with gentle slopes and low elevations, such as valleys and floodplains, are areas where the river flows through.

The vegetation in the watershed is primarily composed of natural forests, shrub lands, and grasslands. The natural forests consist of indigenous tree species such as *Juniperus procera*, *Olea europaea* subsp. *cuspidata*, and *Podocarpus falcatus*. The vegetation cover in the watershed has been significantly impacted by human activities such as deforestation, overgrazing, and agricultural expansion.

Based on the FAO soil classification system, the dominant soil type of the watershed are pellic vertisols (37.54%), chromic vertisols (26.42%), chromic luvisols (21.95%), Eutric nitisols (0.34%), Eutric fluvisols (0.02%), Eutric cambisols (6.83%), Dystric histosols (1.07%), and Leptosols (5.53%), of the watershed total area, respectively. The study area is dominated by clay and sandy clay loam soil textures.

The watershed's yearly rainfall ranges between 815 mm and 1360 mm. The monthly maximum temperature (T_{max}) varies from 21.60°C to 28.72°C, while the monthly minimum temperature (T_{min}) ranges from 9.78°C to 15.62°C.

The research area was chosen because it is one of the primary tributaries of the Genale Dawa basin, and no impact assessment studies on the watershed have been conducted.

Methodology

Data availability

Land use/cover prediction and model validation. The CA-Markov model was selected to predict the 2035 & 2055 LULC change due to its advantage in terms of the capacity of individuals to enhance information under regular principles, governs their evaluation and analysis of spatial (space) features, which may be used to simulate future land usage (Gambo et al., 2018). The CA-Markov model embedded in IDRISI software is used to predict the trend and the spatial structure of distinct LULC categories (S. Li et al., 2015) based on observed LULC image, transition probability matrix and suitability images as a group file (Clark, 2012; Eastman, 2012).

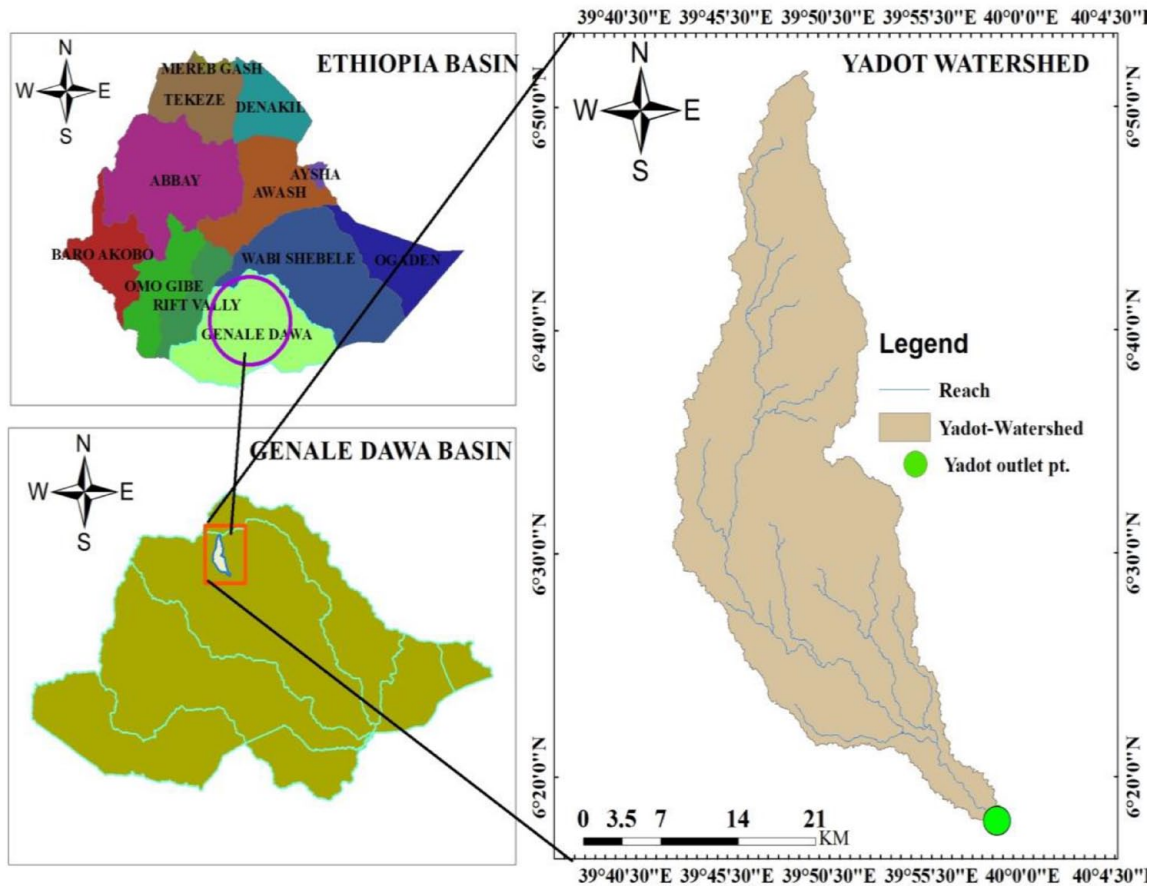


Figure 1. The map showing study area location.

The following procedures were followed to simulate the future LULC changes. (1) the transition probability image was created using LULC maps from 2001 to 2015, (2) the 2015 LULC was calculated using 1985 and 2001 transition probabilities, (3) the multi-criteria assessment module's limitations and factors were used to create the transition suitability image, (4) finally, utilizing the transition probabilities image, base map, and transition suitability image CA-Markov in IDRISI software. The base map, transition probabilities and transition suitability images were used to simulate the 2035 and 2055 LULC changes.

Model calibration and validation are required for every model prediction. Validation is the comparison of the anticipated LULC map to a reference map to determine its quality. To replicate the 2015 LULC picture, LULC photos from 1985 and 2001 were used. The validated module was also used to make comparisons between the simulated and observed LULC class areas.

The CA-Markov model's effectiveness in predicting land use maps was evaluated by the Kappa index Equation 1:

$$\text{Kappa} = \frac{Po - Pc}{1 - Pc} \quad (1)$$

Where P_o is the proportion of accurately simulated cells in the above equation, and P_c is the predicted proportion adjustment

by chance between the simulated and observed maps. When Kappa is 75%, the output maps are in a great agreement; when Kappa is 50%, the output maps are in a medium level of agreement; and when Kappa is 25%, the output maps are in a poor level of agreement; and when Kappa = 1 for perfect agreement (Pontius & Malanson, 2005).

Future climate change projection data

Future climate data, such as daily precipitation, T_{max} and T_{min} are derived from the three dynamically downscaled high-resolution regional climate models CCLM4-8-17, RACMO22T, and RCA4 using RCP 4.5 and RCP 8.5 scenarios. These climate models were chosen based on the recommendations of past studies over East Africa (Endris et al., 2013; Lennard et al., 2018; Tesfaye et al., 2019). The study obtained the data from CORDEX-Africa domain with spatial resolutions of $0.44^\circ \times 0.44^\circ$. Many studies have recommended to apply many model ensemble approaches for capturing large uncertainties in climate projections (Dibaba et al., 2019; Laux et al., 2017; Stanzel et al., 2018). Thus, this study used an ensemble mean of three RCMs (CCLM4-8-17, RACMO22T, and RCA4) derived from three GCMs (HadGM2-ES, MPIESM-LR and ICHEC-EC) as boundary conditions (Table 1).

Table 1. Summaries of GCM and RCM Climate Model Used for This Study.

GCM MODEL	GCM FULL NAME	RCM	RCM FULL NAME	RESOLUTION	CLIMATE CENTER
HadGEM2-ES	Hadley Global Environment Model 2-Earth System	CCLM	Regional Climate Limited-Area Modeling	0.44°	Met Office Hadley Center
MPI-ESM-LR	Coupled Model Version 5	RCA4	Rosby Center Regional Atmospheric Model	0.44°	Max Planck Institute for Meteorology (MPI-M)
EC-EARTH	Irish Center for High-End Computing Earth Consortium	RACMO22T	KNMI Regional Atmospheric Climate Model, version 2.2	0.44°	EC-EARTH Consortium

The projected regional climate data was in the NetCDF file format. ArcGIS10.4.1 software was used to extract rainfall and temperature data from RCMs using a multidimensional tool and a NetCDF table view. The data from the stations was retrieved using their latitudes and longitudes.

The distribution maps of bias corrected future rainfall and temperature data are compared with the baseline data sets (1985–2015). An ensemble of three RCMs was used to predict the change in rainfall and temperature for the near future (2021–2050) and mid-future (2051–2080) periods under RCP4.5 & RCP8.5 scenarios against the baseline (1985–2015) period for the Yadot watershed (Table 1).

Bias correction of RCMs data

This research used power transformation for rainfall and variance scaling methods for temperature as the preferable bias correction methods. These methods have been widely applied for bias adjustment (Fang et al., 2015; Tumsa, 2022). In regional climate models, the power transformation technique was applied to address geographic distributional biases in rainfall outputs. The power transformation equalizes peak daily and monthly precipitation quantities at rain gage sites; the power transformation adjusts the mean and coefficient of variance. Each daily precipitation quantity P is turned into a corrected P^* using this nonlinear adjustment (Equation 2).

$$P^* = aP^b \quad (2)$$

Where P^* is the bias-adjusted daily precipitation, P , the uncorrected daily precipitation and a & b are the transformation coefficients. The b parameter is determined iteratively until the coefficient of variation of the corrected RCM daily precipitation time series equals that of the observed precipitation time series for each grid box in each month. The coefficient a , is calculated using the average of precipitation data and P^b data. Finally, in order to construct the corrected daily time series, monthly constants a and b are applied to each uncorrected daily observation corresponding to that month in order to generate the corrected daily time series

The Variance Scaling approach was created to adjust the mean as well as the variance of regularly distributed variables like temperature (Teutschbein & Seibert, 2012). The Variance Scaling technique is commonly used to adjust temperature (Equation 3).

$$T_c = [T - \mu(T)] \times \frac{\sigma(T_o)}{\sigma(T)} + \mu(T_o) \quad (3)$$

Where T_c is the corrected daily temperature and T is the uncorrected daily temperature from the RCM model; (T_o) is the observed temperature standard deviation and (T) is the uncorrected temperature standard deviation; (T) is the simulated mean temperature and (T_o) is the observed mean temperature.

Hydrological model. The SWAT model is open-source model with a wide and rising number of model applications spanning from watershed to continental dimensions (Arnold et al., 2012; Neitsch et al., 2011). The model divided the watershed into various sub-basins and further segmented into hydrological response units (HRUs) with similar land use management, slope, and soil characteristics (Arnold et al., 2012). HRUs are the basic units of the watershed where important hydrologic components, including evapo-transpiration, surface run-off and peak rate of run-off, groundwater flow, and sediment yield may be calculated.

The major SWAT inputs include Digital Elevation Model (DEM) climate, hydrology, soils and land management. For this study, The DEM, of 12.5 m by 12.5 m was obtained from <https://vertex.daac.asf.alaska.edu/website>. The DEM along with soil and land use/cover data are used to delineate the watershed and to further divide it into sub watersheds and for classification slope, which was the basis in Hydrological Response Unit (HRU) generation (Figure 2).

Soil data was processed from the world digital soil map with a 250 m resolution of soil grids using ArcGIS10.4.1 software (FAO, 2015). The soil classification was customized in the way the SWAT model requires based on the FAO classification system (Figure 2). The dominant soil type of the watershed was pellic vertisols and chromic vertisols covers about 37.84% and 26.42% of the total area, respectively.

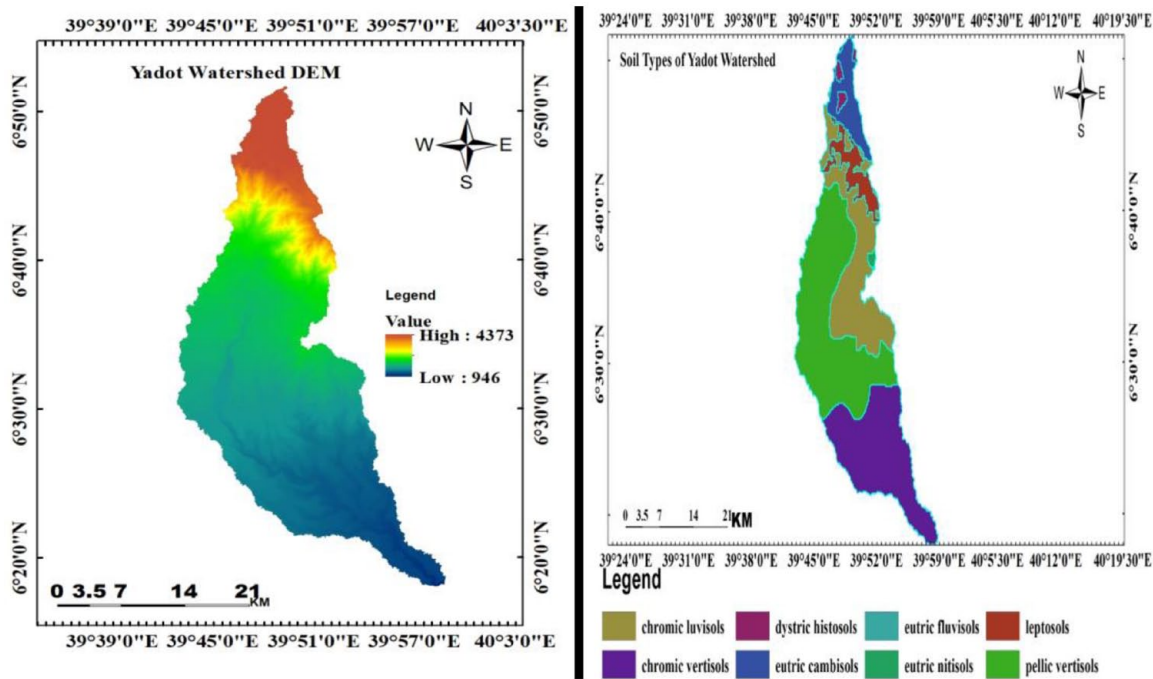


Figure 2. Digital elevation model and soil map of Yadot watershed.

Table 2. Data Source, Location and Time Span of Hydrological and Meteorological Stations.

NO	METEOROLOGICAL STATIONS	DATA SOURCE	LOCATION	TIME
1	Delo Mena (all parameters)	NMAE	Lat: 6.42 & Long: 39.83	1985–2015
2	Rira (all parameters)	NMAE	Lat: 7.02 & Long: 39.83	1985–2015
	Hydrological station			
	Near Delo Mena	MEWRE	Lat: 6.25 N & Long: 39.51E	1985–2008

Note. NMAE = National Meteorological Agency of Ethiopia; MEWRE = Minister of Energy and Water Resources of Ethiopia.

The daily climate variables including daily precipitation (mm), T_{max} and T_{min} (°C), solar radiation (MJ/m²/day), wind speed (m/s) and relative humidity (-) were obtained from two meteorological stations from National Meteorological Service Agency of Ethiopia (Table 2). The observed daily streamflow data of Yadot River at Delo Mena gaging station were obtained from Ministry of Water, Irrigation and Electricity from 1985 to 2008 for calibration and validation.

The LULC maps of 1985, 2001 and 2015 were obtained from Landsat images of TM5, Land sat 7 ETM+, and Land sat 8 OLI, respectively, using ERDAS Imagine 2015 packages. The images were obtained from the USGS (<https://earthexplorer.usgs.gov/>) website. The main land use/cover of the watershed are agricultural lands, grass/range land, forestland, scrub/bush land, woodland and settlement. The dominant LULC in the watershed about 60.45% is covered with forestland and 14.21% with agriculture based on land use/cover map 2015.

Sensitivity analysis, calibration and validation. Sensitivity Analysis. Sensitivity parameters were identified using SUFI 2.

SWAT input settings were calibrated both manually and automatically with SWAT-CUP, software that can perform many iterations for a variety of parameters and determine the best-fit values within a reasonable range (Abbaspour, 2015). SWAT-CUP includes SUFI-2, a sequential uncertainty fitting technique.

Table 3 shows the sensitive parameters for the streamflow predications on Yadot River. The t-stat and p-values were used to quantify sensitive flow parameters. The sensitive parameters were chosen because p-values are nearer to zero and t-stat values are more sensitive to larger absolute t-stat values. Similarly, Negewo and Sarma (2021) found CN2 and SOL K the most sensitive parameters for estimating runoff in the Genale watershed.

Model calibration and validation. The SWAT calibration was done using the observed flow data between 1988 and 2002 years, whereas the validation was done using the observed flow data between 2003 and 2008 years. The years between 1985 and 1987 was used for warming up. The LULC data of 2015 was used for river flow calibration and validation.

Table 3. The Rank and Fitted Value of Sensitive Flow Parameters.

PARAMETER NAME	SENSITIVITY RANK	T-STAT	P-VALUE	MIN VALUE	MAX VALUE	FITTED VALUE
2:V__CANMX.hru	1	-28.82	.00	0.00	20.50	2.70
1:R__CN2.mgt	2	-23.56	.00	-0.18	1.70	-0.12
3:R__SOL_K (. . .).sol	3	12.54	.00	-0.09	0.21	0.20
4:V__ESCO.hru	4	7.44	.00	0.89	0.98	0.98
8:V__CH_K2.rte	5	3.92	.00	30.18	85.08	75.61
6:R__SOL_AWC (. . .).sol	6	3.57	.00	-0.10	0.23	-0.01
10:V__GW_DELAY.gw	7	-1.69	.09	52.19	67.10	61.84
9:V__GWQMN.gw	8	0.43	.67	3,379.73	3,682.36	3,423.16
7:V__ALPHA_BF.gw	9	-0.29	.77	0.65	0.86	0.81
5:V__RCHRG_DP.gw	10	-0.01	.99	0.78	0.89	0.88

Note. A, indicates add the fitted value to the existing value, V implies replace the existing value with the fitted value; R indicates multiply the existing value with (1+ the fitted value).

The SWAT model's performance was evaluated by the coefficient of determination (R^2), Nash–Sutcliffe efficiency (NSE) index, Root mean square error standard deviation ratio (RSR), and the percentage bias (PBIAS). The closer the value of R^2 to one implies a perfect agreement between the simulated and observed flow (Singh et al., 2005).

$$R^2 = \frac{\sum (X_i - X_{av}) * \sum (Y_i - Y_{av})}{\sum \sqrt{(X_i - Y_{av})^2} \sum \sqrt{(Y_i - Y_{av})^2}} \quad (4)$$

Where X_i =measured value (m^3/s); X_{av} =average measured value (m^3/s); Y_i =simulated value (m^3/s) and Y_{av} is average simulated value (m^3/s)

When the value of Nash-Sutcliffe efficiency coefficient (NSE) is 1, the simulated value is the same as observed (perfect) calculated by using Equation 5.

$$ENS = 1 - \frac{\sum (X_i - Y_i)^2}{\sum (X_i - X_{av})^2} \quad (5)$$

Where X_i is measured value; Y_i is simulated value and X_{av} is average observed value.

When the value is between 0 and 1, it indicates the deviations between observed and simulated data. When the efficiency is less than zero, the mean value of the observed time series would be a better predictor than the model result (Krause & Flugel, 2005). The performance indicators based on monthly streamflow values are indicated below (Table 4).

Separate and combined impact of climate and LULC change to stream flow. The streamflow simulation was carried out for near and midterm period under medium and high emission scenarios using projected climate and LULC data as input. The streamflow simulations were carried out under six different

conditions (Table 5): (1) Impact of only predicted LULC during 2035 and 2055 years; (2) Impact of only projected climate during near term (2021–2050) and midterm (2051–2080) periods and with two climate scenarios against 1985 to 2015 baseline data, (3). For the combined impacts of climate and LULC change, there were four simulated scenarios (N_o 3–6) as indicated in Table 5.

Results and Discussion

CA-Markov model performance

The performance assessment of the CA-Markov model was done using the kappa index by comparing the observed and simulated 2015 LULC data through kappa variables. The simulation result showed that the Kappa variation evaluation is as follows: 0.89 for *Kno*, 0.90 for *Klocation*, 0.90 for *Klocation Strata* and 0.84 for *Kstandard*, showing a high level of agreement between the simulated and observed LULC 2015. The performance result showed the effectiveness of the CA-Markov model in simulating the future LULC in the watershed.

Flow calibration and validation. For flow calibration and validation, the actual and simulated flow hydrograph values of the 2015 LULC were created (Figure 3).

The model's performance during the validation period demonstrates a significant correlation and agreement between monthly observed & simulated flow (NSE = .77 and R^2 = .83) (Table 6).

Predicted LULC change

Table 7 presents predicted LULC change between 2035 and 2055 against the baseline LULC. The LULC predictions of 2035 and 2055 were built using the 2015 land use map. The LULC data between 2001 and 2015 were used to develop the

Table 4. SWAT Model Performance Indicators Based on Monthly Streamflow Values.

PERFORMANCE RATING	R^2	NSE	PBIAS (%)	RSR
Very good	$0.86 < R^2 \leq 1$	$0.75 < NSE \leq 1$	$PBIAS < 10$	$0.0 \leq RSR \leq 0.5$
Good	$0.75 < R^2 \leq 0.86$	$0.65 < NSE \leq 0.75$	$10 \leq PBIAS < 15$	$0.5 < RSR \leq 0.6$
Satisfactory	$0.65 < R^2 \leq 0.75$	$0.5 < NSE \leq 0.65$	$15 \leq PBIAS < 25$	$0.6 < RSR \leq 0.7$
Un satisfactory	$R^2 \leq 0.65$	$NSE \leq 0.5$	$PBIAS \geq 25$	$RSR \geq 0.7$

Table 5. LULC and Climate Change Simulation Results.

NO	SIMULATED PROJECTED IMPACT	INPUTS FOR SIMULATION
1	Impact of only predicted LULC change	Predicted LULC of 2035 & 2055 with baseline climatic data of 1985–2015
2	Impact of only projected climate change	Projected climate 2021–2050 & 2051–2080 with baseline LULC data of 2015
3	Impact of combined projected near-term climate and predicted LULC change during 2035 under medium climate scenario (RCP4.5)	Near-term climate projection (2021–2050) and 2035 LULC prediction using RCP4.5 climate scenario
4	Impact of combined projected near-term climate and predicted LULC change during 2035 under high climate scenario (RCP8.5)	Near-term climate projection (2021–2050) and 2035 LULC prediction under RCP8.5 climate scenario
5	Impact of combined projected mid-term climate and predicted LULC change during 2055 under medium climate scenario (RCP4.5)	Mid-term climate projection (2051–2080) and 2055 LULC prediction under RCP4.5 climate scenario
6	Impact of combined projected mid-term climate and predicted LULC change during 2055 under high climate scenario (RCP8.5)	Mid-term climate projection (2051–2080) and 2055 LULC prediction under RCP4.5 climate scenario

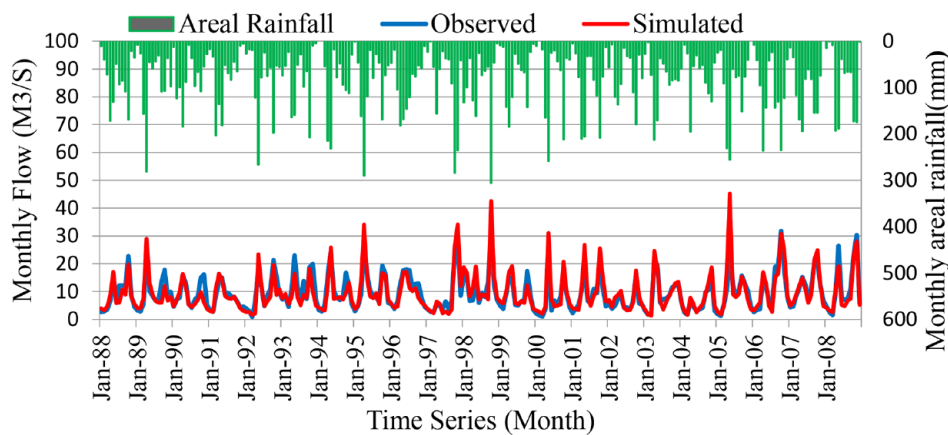


Figure 3. Calibrated and validated streamflow values against areal rainfall.

transition matrix and transfer probability matrix. The predicted LULC changes between 2015 and 2035 showed that agricultural land, grassland, settlement areas and woodland increase by 17.09%, 32.38%, 43.38% and 75.05%, respectively. Similarly, the projected LULC change between 2015 and 2055 showed agricultural land, grassland, settlement areas and woodland increase by 44.02%, 30.35%, 69.2% and 55.05%, respectively. The forest and scrub/bush lands decreased between 2015 and 2035 by 18.26% and 10.72%, respectively. Similarly, the forest and scrub/bush land decreased between 2015 and 2055 by 21.53% and 11.08%, respectively.

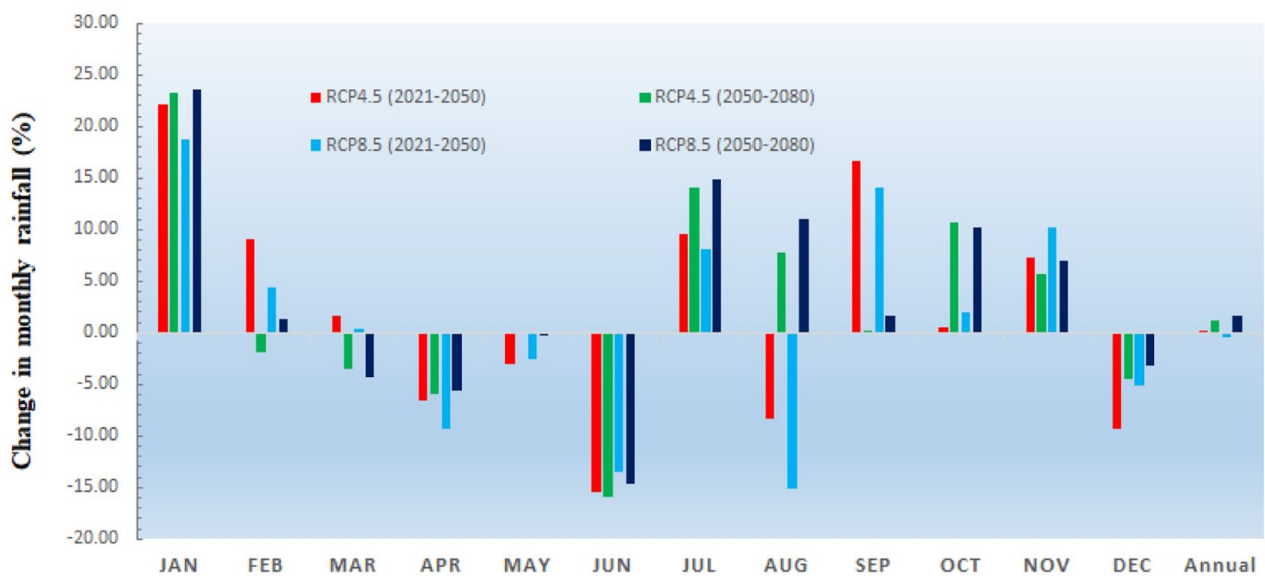
Generally, the predicted future LULC change pattern indicated that agricultural land, grassland, settlement areas and woodlands showed consistent increase both under 2035 and 2055 periods. The predicted future LULC changes are linear with the past *pattern of change*. The woodland exhibited the largest increase (75.05%) between 2015 and 2035 years. The overall, increase in woodland may be attributable to government-planned afforestation efforts and green legacy initiatives. The projected woodland increase could be positive in its effect to water resources whereas the increase in agricultural land, grassland and settlement areas tend to have a *negative effect* on

Table 6. Performance Indicators for SWAT Model Calibration and Validation.

PERIODS	MODEL PERFORMANCE EVALUATION CRITERIA					
	R ²	NSE	% PBIAS	RSR	P-FACTORS	R-FACTORS
Calibration (1988–2002)	0.80	0.73	16.1	0.52	0.76	0.81
Validation (2003–2008)	0.83	0.77	11.2	0.48	0.82	0.79

Table 7. Predicted LULC Change During the Two Future Periods 2035 & 2055 Against the Historical LULC of 2015 for Yadot Watershed.

LULC	HISTORICAL LULC 2015	PREDICTED LULC CHANGE (%)	
	AREA (HA)	CHANGE (%) BETWEEN 2015 AND 2035	CHANGE (%) BETWEEN 2015 AND 2055
Agriculture	10,453.35	17.09	44.02
Forest	45,200.12	-18.26	-21.53
Grass/Range	5,366.55	32.38	30.35
Scrub/Bush	5,253.04	-10.72	-11.08
Settlement	537.41	43.38	69.2
Wood land	6,742.77	75.05	55.05

**Figure 4.** Change in mean monthly and annual rainfall for near (2021–2050) and mid-term (2051–2080) periods under both scenarios in the Yadot watershed.

water resources due to their effect on vegetation cover. Because, LULC change is mainly dominated by the conversion of natural vegetation cover to use for agriculture activities in Ethiopia (Gashaw et al., 2018a). Similarly, several research works have shown that there has been a significant LULC change in different parts of the country dominated by the expansion of cultivated land and built-up areas at the expense of natural vegetation cover, shrublands, which is consistent with our findings (Deribew & Dalacho, 2019; Dibaba et al., 2020b; Yesuph & Dagne, 2019).

Climate change projections

Rainfall projections. Figure 4, presents monthly and annual rainfall percentage change for near term (2021–2050) and midterm (2051–2080) projection periods under RCP4.5 & RCP8.5 scenarios. The change in projected mean monthly rainfall showed mixed results in relation to magnitude and direction of change during near-term and midterm periods and under both scenarios. The projected mean monthly rainfall increased in the months of January, July, September, October and November during near and midterm projection periods

Table 8. Change in Wet and Dry Season Rainfall Projection During Near and Midterm Period Under RCP4.5 & RCP8.5 Scenarios in Yadot Watershed.

SEASONS	BASELINE PERIOD	NEAR-TERM PERIOD		MID-TERM PERIOD	
	RAINFALL (MM)	SCENARIOS		SCENARIOS	
		RCP4.5	RCP8.5	RCP4.5	RCP8.5
		% CHANGE	% CHANGE	% CHANGE	% CHANGE
Wet season	917.92	0.02	-0.62	1.34	1.59
Dry season	141.67	0.85	0.59	0.7	2.08

under both scenarios. The highest projected rainfall increase was 23.55% in the month of January during midterm period under RCP8.5 scenarios. The projected rainfall increase during the months of January, July, September, October and November ranges between 0.21% and 23.55%.

However, the change in projected mean monthly rainfall decreased during the months of April, May, June and December during both near-term and midterm periods under both scenarios. The decrease in projected mean monthly rainfall during those months range between 2.50% and 15.43%.

The mean annual rainfall during near and midterm periods predicted to rise by 0.13% and 1.25%, respectively, under RCP4.5 scenario. The mean annual rainfall during near-term period showed a minor decline by 4.85 mm under RCP8.5 scenario, while it increased by 1.66% during midterm period under same scenario. Thus, the mean annual rainfall increased under both periods and scenarios except during the near-term period under RCP 8.5 scenario.

The change in seasonal rainfall projection slightly increased during both wet (March, April, May, August, September, October and November) and dry (January, February, June, July and December) seasons in the range of 0.02%–2.08% during both near and midterm periods under both RCP 4.5 and RCP8.5 scenarios (Table 8). However, wet season rainfall slightly decreased by 0.62% during near term period under RCP8.5 scenario.

The change in seasonal rainfall projection slightly increased during both the wet (March, April, May, August, September, October and November) and dry (January, February, June, July and December) seasons in the range of 0.02%–2.08% during near and mid-term periods under both RCP 4.5 and RCP8.5 scenarios (Table 8).

Similar studies conducted on various parts of Ethiopia support our findings. For instance, Gizaw et al. (2017) reported, the projected mean annual rainfall increase in Awash, Baro, Genale, and Tekeze river basins of Ethiopia. Recently, Birhan et al. (2021) reported 25% rainfall rise in Lake Tana Sub-basin. A similar study by Bekele et al. (2021) in the Arjo-Didessa catchment, upper Blue Nile basin, projected the annual rainfall to increase by 0.36 to 2% during the medium future (2041–2070) under RCP 4.5 scenario.

Temperature projections. Figure 5a and b, Presents change in projected mean annual and monthly T_{max} and T_{min} during near-term and midterm period under both emission scenarios. The projected near-term mean monthly maximum temperature increased from June–September under both scenarios. However, the mean monthly maximum temperature decreased between February and March during the same period and under both scenarios. The projected near-term mean monthly minimum temperature during the months of June, February, September, October, November, and December increased under both scenarios. The months with a decreased mean minimum temperature for the near-term period under both scenarios, however, are during the months of March, April, May, June, and July. The largest increased projected near-term mean monthly maximum temperature was 3.42°C on October under RCP4.5 scenario and minimum temperature was 3.74°C on January under RCP8.5 scenarios.

Generally, the projected mid-term mean monthly maximum temperature increased in all months under both scenarios (RCP4.5 & RCP8.5) except during January, February, March, November and December months where the mean monthly T_{max} increased under RCP4.5 scenario. Similarly, the projected mid-term mean monthly minimum temperature increased in all months under both scenarios except during the months of October, November, and December, where the mean monthly minimum temperature increased under RCP4.5 scenario. The highest projected midterm mean monthly maximum temperature increase was 5.61°C on July under RCP4.5 scenario and minimum temperature was 3.89°C on June under RCP8.5 scenarios.

The mean maximum and minimum temperatures increased during both near and midterm periods under both scenarios (Figure 5). The highest projected mean annual maximum and minimum temperature was 2.0°C and 1.8°C, respectively during mid-term period under RCP8.5 scenario (Figure 5).

The wet and dry season maximum and minimum temperature increased during both the near and mid-term period under the two emission scenarios (Table 9). The magnitude of seasonal maximum temperature increase is highest (2.07°C) on wet season during mid-term period under RCP8.5scenarios. The magnitude of seasonal minimum temperature increase is

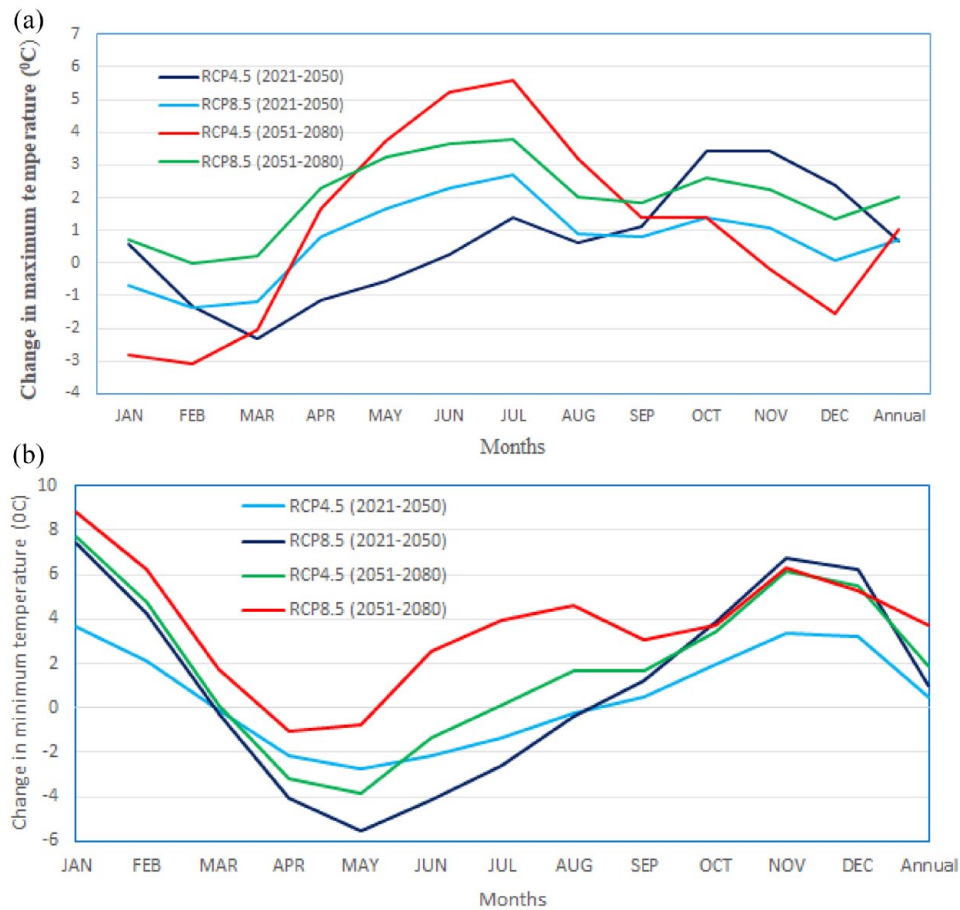


Figure 5. Change in mean annual and monthly: (a) maximum and (b) minimum temperatures ($^{\circ}\text{C}$) during near-term (2021–2050) and mid-term (2051–2080) period under RCP4.5 and RCP8.5 scenarios in the Yadot watershed.

Table 9. Change in Mean Seasonal T_{max} and T_{min} During Near & Mid-Term Period Under Both Scenarios.

SEASONS	BASELINE		NEAR-TERM PERIOD (2021–2050)				MID-TERM PERIOD (2051–2080)			
	OBSERVED	OBSERVED	RCP4.5	RCP8.5	RCP4.5	RCP8.5	RCP4.5	RCP8.5	RCP4.5	RCP8.5
	T_{MAX} ($^{\circ}\text{C}$)	T_{MIN} ($^{\circ}\text{C}$)	CHANGE	CHANGE	CHANGE	CHANGE	CHANGE	CHANGE	CHANGE	CHANGE
		T_{MAX} ($^{\circ}\text{C}$)	T_{MAX} ($^{\circ}\text{C}$)	T_{MIN} ($^{\circ}\text{C}$)	T_{MIN} ($^{\circ}\text{C}$)	T_{MAX} ($^{\circ}\text{C}$)	T_{MAX} ($^{\circ}\text{C}$)	T_{MIN} ($^{\circ}\text{C}$)	T_{MIN} ($^{\circ}\text{C}$)	
Wet season	28.62	16.21	0.65	0.78	0.06	0.14	1.31	2.07	0.65	1.66
Dry season	28.88	15.39	0.65	0.61	1.07	1.14	0.68	1.90	1.13	2.01

highest (2.01°C) on dry season during mid-term period under RCP8.5 scenario.

Generally, annual and seasonal temperature has consistently increased for both periods and climate scenarios. However, monthly temperature results indicated both decreasing and increasing projected trends. The highest projected maximum and minimum temperature increase was obtained under RCP 8.5 scenarios.

This result agrees with previous studies in Ethiopia that reported a consistent increasing trend of projected T_{max} and T_{min} for all time horizons, with a higher rate of increase at the

end of 21st century (Chakilu et al., 2020; Gurara et al., 2023; Dibaba et al., 2020a; Worqlul et al., 2018).

Predicted LULC change impact on streamflow. Table 10 presents changes in seasonal and annual streamflow (M^3/s) under predicted LULC change against baseline climate. The mean annual streamflow increased by 0.64% ($3.74 \text{ m}^3/\text{s}$) and 1.19% ($6.93 \text{ m}^3/\text{s}$) under the 2035 & 2055 predicted LULC change, respectively as compared to the 2015 historical LULC. The mean annual streamflow increment could be attributed to the expected expansion of agricultural and settlement area and due to the continued removal of plant cover.

Table 10. Change in Annual & Seasonal Streamflow (M3/s) Under Predicted LULC Change Using Baseline Climate.

SEASONS	STREAMFLOW UNDER HISTORICAL LULC (M3/S)	STREAMFLOW UNDER PREDICTED LULC (M3/S)	STREAMFLOW UNDER PREDICTED LULC (M3/S)
	2015	2035	2055
Annual	581.14	0.64	1.19
Wet season	416.98	1.47	2.90
Dry season	164.15	-1.44	-3.14

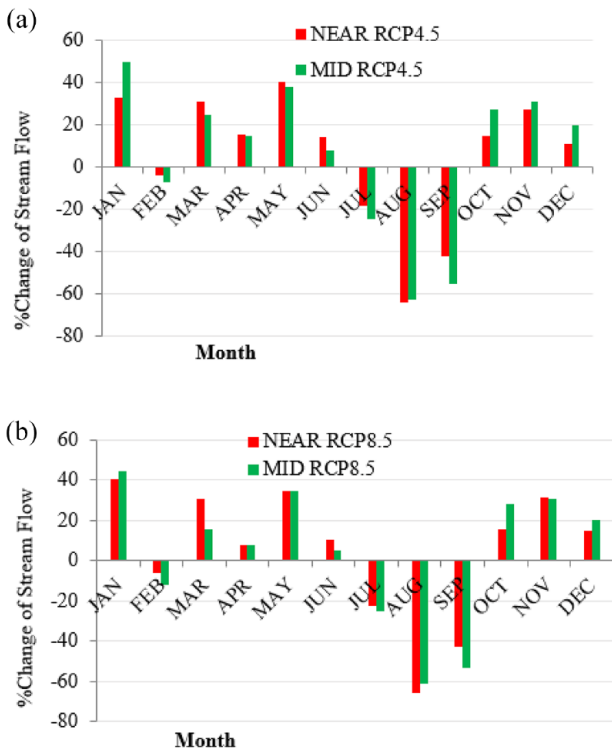


Figure 6. Change in flow percentage in the near and midterm period under RCP4.5 scenario (a) and RCP 8.5 scenario (b) compared to the baseline period.

The wet season streamflow increased by 1.47% (6.12 m³/s) and by 2.9% (12.1 m³/s) under the 2035 & 2055 predicted LULC change, respectively as compared to the 2015 historical LULC. However, the dry season streamflow decreased by 1.44% (2.36 m³/s) and by 3.14% (5.16 m³/s) under the 2035 & 2055 predicted LULC change, respectively as compared to the 2015 historical LULC

Surface runoff contributed more to streamflow during rainy months than groundwater did during dry season. Wet season flow is less responsive to LULC change throughout the LULC projected period than dry season flow because ground water input during the dry season decreased due to less infiltration, which mostly resulted in less plant cover. The growth of wooded and grassy areas together with an uptick in agriculture and habitation led to a larger rate of streamflow increment for the past LULC than for the future LULC. This result is in line with other previous studies. For instance, Gashaw et al. (2018b)

found that due to LULC change in the Upper Blue Nile Basin, annual and wet season flow and surface runoff increased while dry season flow, decreased between 1985 and 2015. The outcome also demonstrates that for LULC 2030 and 2045, flow is expected to grow yearly during the wet season, whereas flow is projected to decline during the dry season. According to Rajib and Merwade (2017) calculations, the average annual streamflow at the basin outflow will rise for the future LULC during the years 2081 to 2100, respectively.

Projected climate change impact on streamflow. Figure 6a and b, presents the near-term and midterm mean monthly streamflow changes (%) under the RCP4.5 and RCP8.5 scenarios. Except the months July, August, and September, which showed a streamflow decline, all the months indicated mean monthly streamflow rise during the near-term and midterm period under both scenarios. This result indicates that the months of August and September would be severely impacted during the near and midterm period under both scenarios (Figure 6). Under both scenarios emission scenarios, the overall trend indicates that the streamflow will generally rise on an annual, seasonal, and monthly basis.

Studies by Negewo and Sarma (2021) reported that mean annual streamflow consistently increased with the predicted changes in rainfall and temperature patterns in the future period 2022 to 2080 under both emission scenarios of the Genale watershed, which is consistent with the projected increase in streamflow into the watershed. In the same vein, Adem et al. (2016) concluded that the mean annual streamflow projections increase during the 2020s, 2050s, and 2080s under A2 climate scenarios. Therefore, the variation in mean streamflow for wet and dry seasons that would occur from climate change impacts in the Bale highlands affect not only the quality of life for those who reside in the Bale zone but also all those whose way of life rely on the Yadot River.

Table 11 presents changes in projected seasonal and annual streamflow (M³/s) during near and mid-term period under both scenarios & using historical LULC change (2015). The projected mean annual streamflow showed an increase by 7.63% and 5.76% under the RCP4.5 and RCP8.5 scenarios, respectively during the near-term period. Similarly, the mean annual streamflow is expected to rise by 8.25% and 6.07%, under RCP4.5 and RCP8.5 scenarios, respectively during the midterm period.

Table 11. Changes in Projected Seasonal and Annual Streamflow (M³/s) During Near and Mid-Term Climate Projection Period Under RCP4.5 and RCP8.5 Scenarios With Historical LULC Change (2015).

SEASONS	BASELINE SIMULATED STREAMFLOW IN (M ³ /S)	% CHANGE OF STREAMFLOW			
		RCP4.5		RCP8.5	
		NEAR-TERM	MID-TERM	NEAR-TERM	MIDTERM
Annual	581.14	7.63	8.25	5.76	6.07
Wet season	416.99	8.48	9.36	6.23	7.21
Dry season	164.15	5.46	5.41	4.57	3.16

For the wet (March to May and August to November) and dry (January, February, June, July, and December) seasons, the seasonal variation of the expected streamflow from the baseline period was estimated. In the near future period, the mean streamflow during the wet season is expected to rise from the baseline flow by 8.48% and 6.23% under RCP4.5 and RCP8.5 scenarios, respectively. In the midterm period, the mean streamflow during the wet season might rise by 9.36% and 7.21% under RCP4.5 and RCP8.5 scenarios, respectively (Table 11). In the near future period, the mean streamflow during the dry season are likely to rise from baseline flow by 5.46% and 4.57% under the RCP4.5 and RCP8.5 scenarios, respectively. Similarly, in the midterm period, the mean dry season streamflow is expected to increase by 5.41% and 3.16% under the RCP4.5 and RCP8.5 scenarios, respectively. Understanding the future changes in streamflow during the wet and dry seasons is crucial to assessing the hydrological effects of climate change.

Combined impact of climate and LULC change on streamflow. The maximum mean monthly change of flow increment was seen in May by 39.4% (35.39 m³/s) and 35.36% (31.77 m³/s) from the baseline period, while the minimum mean monthly change of flow increment was seen in December and March by 5.87 m³/s (15.81%) and 2.3 m³/s (11%), respectively (Figure 7).

The integrated impact of climate and LULC change indicated a decline in mean monthly streamflow on February, July, August and September months under both scenarios and projection periods. However, all the remaining months showed an increase in monthly streamflow under both scenarios and projection periods.

In the near-term period, the projected mean annual streamflow increased by 8.13% and 6.26% under the RCP4.5 and RCP8.5 scenarios, respectively. Similarly, during the mid-term period, the projected mean annual streamflow increased by 8.96% and 6.77% under the RCP4.5 and RCP8.5 scenarios, respectively (Table 12). The modest decline in mean annual streamflow from RCP4.5 to RCP8.5 scenario could likely be attributed to annual and seasonal decline in precipitation from the baseline period together with a rise in temperature throughout the watershed.

The wet and dry season streamflow projection showed a consistent increase during both near and midterm periods

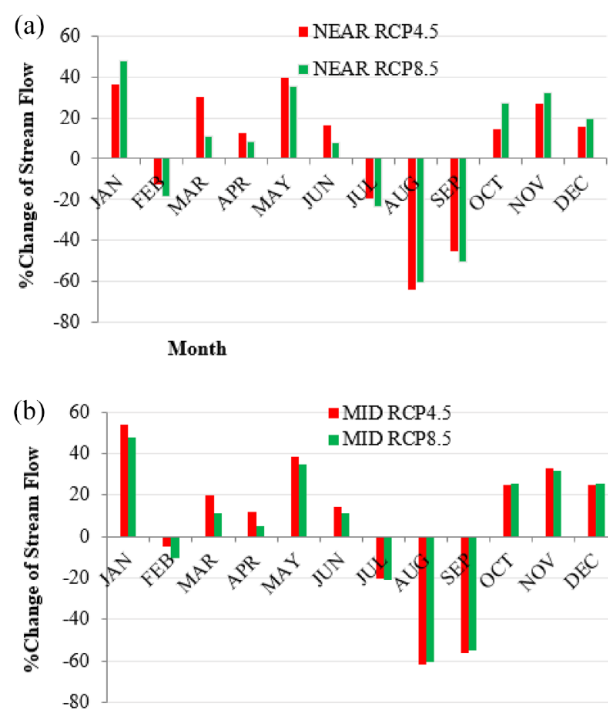


Figure 7. Percentage change of flow for near-term and midterm period under RCP 4.5 scenarios (a) and RCP 8.5 scenarios (b).

under both climate scenarios. If all other factors remain constant, therefore, under both RCP scenarios, mean streamflow during both the wet and dry seasons could rise during the next century. A rise in river flow, therefore, could be expected because of climate and LULC change, but the consequences associated with this should be adequately planned for and minimized, according to modeling results.

When we compared the impact of future climate and LULC changes on streamflow, climate change impact showed a greater influence. This is because streamflow is more responsive to climate change than to changes in LULC. The combined impact showed higher streamflow changes than under only LULC change and climate change.

The results of this study agrees with other climate impact studies conducted at small and large areal scales. For instance, a study by Birhan et al. (2021) reported an increasing streamflow trend under combined climate and LULC change scenarios, due to temperature and precipitation increase in the Lake Tana

Table 12. Change in Mean Annual and Seasonal Streamflow During Near and Mid-Term Period Under Both Scenarios for Combined Climate and LULC Change.

SEASONS	BASELINE STREAMFLOW SIMULATION (M3/S)	% CHANGE OF STREAMFLOW			
		NEAR-TERM CLIMATE PROJECTION WITH 2035 LULC PREDICTION		MIDTERM CLIMATE PROJECTION WITH 2055 LULC PREDICTION	
		RCP4.5	RCP8.5	RCP4.5	RCP8.5
Annual	581.14	8.13	6.26	8.96	6.77
Wet season	416.99	8.72	6.46	8.39	6.25
Dry season	164.15	6.62	5.76	10.42	8.07

Basin, upper Blue Nile River Basin. The Kesem sub-basin of the Awash River basin had a similar analysis that revealed an increase in mean annual streamflow under both scenarios concurrent with increases in rainfall and temperature from the 2050s to 2080 timeframe (Tessema et al., 2021). Similarly, Dagnenet Fenta et al. (2018) indicated that under future climate, the predicted LULC change, and under the combined projection, streamflow and lateral flow reported to rise by up to 25% in the Upper Blue Nile River Basin. A similar study from Pakistan by Babur et al. (2016) reported the mean annual flow increase between the years 2011 & 2040, 2041 & 2070, and 2071 & 2100 under both scenarios. However, there are contradictory findings that reported the decline in streamflow under the combined impact of climate change and LULCC in Fincha, Bilate, Meki watersheds of Ethiopia (Dibaba et al., 2020a; Kuma et al., 2021; Yifru et al., 2021). Generally, this study and previous studies demonstrated that the magnitude of the change of stream flow due to climate and land use and land cover change varies from basin to basin depending on the basin characteristics such as geography, geology, topography, climate conditions, and intensity of land cover changes (Wedajo et al., 2022). Hydrological responses to land cover and climate changes varies from region to region and can exhibit spatiotemporal variability even within a basin (Luo et al., 2016). Thus, understanding the separate and combined impacts of climate and LULC change on streamflow on annual and seasonal basis at different spatial scales are the base to formulate and implement sustainable land and water resource management strategies at different spatial scales.

Conclusions

The LULC prediction results showed that by 2035 & 2055, agricultural land, grassland, settlement areas and woodland will increase while there will be major decreases in scrub/bush land and forestlands. These predicted changes in LULC contributed to the projected annual and wet season streamflow increase while it contributes to a decrease for a dry season streamflow.

The mean annual rainfall is projected to increase during the near and midterm period under both scenarios. The wet and dry season rainfall projections exhibited similar increasing

tendency. However, the mean monthly rainfall projections showed mixed results, with April, May, June and December months projected consistent decrease whereas the remaining months showed an increasing tendency.

The temperature projection consistently indicated a warmer future, as is the case from other several previous studies. The highest mean annual projected temperature was 2.0°C under RCP8.5 scenario during the midterm period. The previous studies in Ethiopia reported a consistent increasing trend of T_{max} and T_{min} during all time horizons in the future.

The streamflow response to the projected climate change was a consistent increase of flow. Overall, the streamflow projections indicated large *streamflow increase annually and during both wet and dry seasons under both scenarios*. When we compared the impact of LULC change and climate change on streamflow, it is obvious that the latter had a greater influence and increased streamflow relative to the baseline period. This is because streamflow is more responsive to climate change than to changes in LULC. The dry season flow has a higher midterm growth tendency than the rainy season flow. In general, the outcome of projected streamflow in the future indicates that the combined LULC and climate change impact on streamflow were somewhat greater than climate change alone. Thus, in the future climate change will be the primary driver of future streamflow than LULC.

Acknowledgements

The authors are grateful to the Ethiopian Ministry of Water and Energy and the Ethiopian National Meteorological Agency for providing streamflow and meteorological data for the Yadot River Watershed, Genale Dawa Basin.

Funding

The author(s) received no financial support for the research, authorship, and/or publication of this article.

Declaration of Conflicting Interests

The author(s) declared no potential conflicts of interest with respect to the research, authorship, and/or publication of this article.

REFERENCES

- Abbaspour, K. (2015). SWAT-CUP 2012: SWAT calibration and uncertainty programs: A user manual. 772 Department of Systems Analysis, Integrated Assessment and Modelling (SIAM), Eawag, Swiss Federal 773 Institute of Aquatic Science and Technology, Duebendorf, Switzerland.
- Abera, W., Tamene, L., Abegaz, A., & Solomon, D. (2019). Understanding climate and land surface changes impact on water resources using Budyko framework and remote sensing data in Ethiopia. *Journal of Arid Environments*, 167, 56–64.
- Aboelnour, M., Gitau, M. W., & Engel, B. A. (2019). Hydrologic response in an urban watershed as affected by climate and land-use change. *Water*, 11(8), 1603.
- Anand, J., Gosain, A. K., & Khosa, R. (2018). Prediction of land use changes based on land change modeler and attribution of changes in the water balance of Ganga basin to land use change using the SWAT model. *The Science of the Total Environment*, 644, 503–519.
- Adem, A., A., Seifu, A., Essayas, K., Abeyou, W., Tewodros, T., Shimelis, B., & Assefa, M. (2016). Climate change impact on streamflow in the upper Gilgel Abay catchment, Blue Nile Basin, Ethiopia. In A. Melesse & W. Abtew (Eds.), *Landscape dynamics, soils and hydrological processes in varied climates* (pp. 645–673). Springer Geography. https://doi.org/10.1007/978-3-319-18787-7_29
- Arnold, J. G., Moriasi, D. N., Gassman, P. W., Abbaspour, K. C., White, M. J., Srinivasan, R., Santhi, C., Harmel, R. D., Van Griensven, A., Van Liew, M. W., & Kannan, N. (2012). SWAT: Model use, calibration, and validation. *Transactions of the ASABE*, 55(4), 1491–1508.
- Azari, M., Moradi, H. R., Saghaifan, B., & Faramarzi, M. (2016). Climate change impacts on streamflow and sediment yield in the north of Iran. *Hydrological Sciences Journal*, 61(1), 123–133.
- Babur, M., Babel, M. S., Shrestha, S., Kawasaki, A., & Tripathi, N. K. (2016). The impact of climate change on reservoir inflows using multi climate-model under RCPs' including extreme events-A case of Mangla Dam, Pakistan. *Water*, 8, 389.
- Bekele, W. T., Haile, A. T., & Rientjes, T. (2021). Impact of climate change on the streamflow of the Arjo-Didessa catchment under RCP scenarios. *Journal of Water and Climate Change*, 12(6), 2325–2337.
- Birhan, G., Manjunatha, B. R., & Bhat, H. G. (2021). Modeling projected impacts of climate and land use/land cover changes on hydrological responses in the Lake Tana Basin, upper Blue Nile River Basin, Ethiopia. *Journal of Hydrology*, 595, 125974.
- Chakilu, G. G., Sándor, S., & Zoltán, T. (2020). Change in stream flow of Gumara watershed, upper Blue Nile Basin, Ethiopia under representative concentration pathway climate change scenarios. *Water*, 12(11), 3046.
- Chang, J., Ciaia, P., Viovy, N., Vuichard, N., Sultan, B., & Soussana, J. F. (2015). The greenhouse gas balance of European grasslands. *Global Change Biology*, 21(10), 3748–3761.
- Clark, L. (2012). *Idrisi Selva help system*. Clark University.
- Clerici, N., Cote-Navarro, F., Escobedo, F. J., Rubiano, K., & Villegas, J. C. (2019). Spatio-temporal and cumulative effects of land use-land cover and climate change on two ecosystem services in the Colombian Andes. *The Science of the Total Environment*, 685, 1181–1192.
- Dagnenet Fenta, Z., Duan, Z., Rientjes, T., & Disse, M. (2018). Analysis of combined and isolated effects of land-use and land-cover changes and climate change on the upper Blue Nile River basin's streamflow. *Hydrology and Earth System Sciences*, 22(12), 6187–6207.
- Deribew, K. T., & Dalacho, D. W. (2019). Land use and forest cover dynamics in the north-eastern Addis Ababa, central highlands of Ethiopia. *Environmental Systems Research*, 8(1), 1–18.
- Dibaba, W. T., Demissie, T. A., & Miegel, K. (2020a). Watershed hydrological response to combined land Use/Land cover and climate change in Highland Ethiopia: Finchaa catchment. *Water*, 12, 1801.
- Dibaba, W. T., Demissie, T. A., & Miegel, K. (2020b). Drivers and implications of land use/land cover dynamics in Finchaa catchment, northwestern Ethiopia. *Land*, 9(4), 113.
- Dibaba, W. T., Miegel, K., & Demissie, T. A. (2019). Evaluation of the CORDEX regional climate models performance in simulating climate conditions of two catchments in Upper Blue Nile Basin. *Dynamics of Atmospheres and Oceans*, 87, 101104.
- Eastman, J. (2012). *IDRISI Selva manual, version 17* (p. 322). Clark University.
- Endris, H. S., Omondi, P., Jain, S., Lennard, C., Hewitson, B., Chang'a, L., Awange, J. L., Dosio, A., Ketiem, P., Nikulin, G., Panitz, H. J., Büchner, M., Stordal, F., & Tazalika, L. (2013). Assessment of the performance of CORDEX regional climate models in simulating East African rainfall. *Journal of Climate*, 26(21), 8453–8475.
- FAO. (2015). World Reference Base for Soil Resources 2014. International Soil Classification System for Naming Soils and Creating Legends for Soil Maps. Update, Rome. <http://www.fao.org/3/a-i3794e.pdf>
- Fang, G. H., Yang, J., Chen, Y. N., & Zammit, C. (2015). Comparing bias correction methods in downscaling meteorological variables for a hydrologic impact study in an arid area in China. *Hydrology and Earth System Sciences*, 19, 2547–2559.
- Gambo, J., Mohd Shafri, H. Z., Shaharum, N. S. N., Abidin, F. A. Z., & Rahman, M. T. A. (2018). Monitoring and predicting land use-land cover (LULC) changes within and around Krau wildlife reserve (KWR) protected area in Malaysia using multi-temporal Landsat data. *Geopanning Journal of Geomatics and Planning*, 5(1), 17–34.
- Gashaw, T., Tulu, T., Argaw, M., & Worqlul, A. W. (2018a). Modeling the hydrological impacts of land use/land cover changes in the Andassa watershed, Blue Nile Basin, Ethiopia. *The Science of the Total Environment*, 619–620, 1394–1408.
- Gashaw, T., Tulu, T., Argaw, M., Worqlul, A. W., Tolessa, T., & Kindu, M. (2018b). Estimating the impacts of land use/land cover changes on ecosystem service values: The case of the Andassa watershed in the Upper Blue Nile basin of Ethiopia. *Ecosystem Services*, 31, 219–228.
- Gebrechorkos, S. H., Taye, M. T., Birhanu, B., Solomon, D., & Demissie, T. (2023). Future changes in climate and hydroclimate extremes in East Africa. *Earth's Future*, 11, e2022EF003011. <https://doi.org/10.1029/2022ef003011>
- Gizaw, M. S., Biftu, G. F., Gan, T. Y., Moges, S. A., & Koivusalo, H. (2017). Potential impact of climate change on streamflow of major Ethiopian rivers. *Climatic Change*, 143(3–4), 371–383.
- Grag, T., Kebede, A., & Berhanu, S. (2019). Evaluation of climate change impacts on the water resources of Awata River Watershed, Genale Dawa Basin: Southern Ethiopia. *Academic Research Journal of Agricultural Science and Research*, 7, 414–422.
- Gurara, M. A., Jilo, N. B., & Tolche, A. D. (2023). Modelling climate change impact on the streamflow in the Upper Wabe Bridge watershed in Wabe Shebe River Basin, Ethiopia. *International Journal of River Basin Management*, 21(2), 181–193.
- Hyandye, C. B., Worqul, A., Martz, L. W., & Muzuka, A. N. N. (2018). The impact of future climate and land use/cover change on water resources in the ndembera watershed and their mitigation and adaptation strategies. *Environmental Systems Research*, 7(1), 1–24.
- IPCC. (in press). Climate change and land: An IPCC special report on climate change, desertification, land degradation, sustainable land management, food security, and greenhouse gas fluxes in terrestrial ecosystems. In P. R. Shukla, J. Skea, E. Calvo Buendia, V. Masson-Delmotte, H.-O. Pörtner, D. C. Roberts, P. Zhai, R. Slade, S. Connors, R. van Diemen, M. Ferrat, E. Haughey, S. Luz, S. Neogi, M. Pathak, J. Petzold, J. Portugal Pereira, P. Vyas, E. Huntley, J. Malley, et al. (Eds.).
- IPCC. (2013). Summary for Policymakers. In T. F. Stocker, D. Qin, G.-K. Plattner, M. Tignor, S. K. Allen, J. Boschung, A. Nauels, Y. Xia, V. Bex, & P. M. Midgley (Eds.), *Climate change 2013: The physical science basis. Contribution of working group I to the Fifth assessment report of the intergovernmental panel on climate change*. Cambridge University Press.
- Koch, H., Biewald, A., Liersch, S., Azevedo, J. R. G. D., Silva, G. N. S. D., Kölling, K., Fischer, P., Koch, R., & Hattermann, F. F. (2015). Scenarios of climate and land-use change, water demand and water availability for the São Francisco River Basin. *Brazilian Journal of Environmental Sciences*, 36, 96–114.
- Krause, P., & Flugel, W. A. (2005). Integrated research on the hydrological process dynamics from the Wilde Gera catchment in Germany; Headwater Control VI: Hydrology, Ecology and Water Resources in Headwaters, IAHS Conference, Bergen
- Kuma, H. G., Feyessa, F. F., & Demissie, T. A. (2021). Hydrologic responses to climate and land-use/land-cover changes in the bilate catchment, southern Ethiopia. *Journal of Water and Climate Change*, 12, 3750–3769.
- Laux, P., Nguyen, P. N. B., Cullmann, J., Van, T. P., & Kunstmann, H. (2017). How many RCM ensemble members provide confidence in the impact of Land-Use land cover change? *International Journal of Climatology*, 37, 2080–2100.
- Lennard, C. J., Nikulin, G., Dosio, A., & Moufouma-Okia, W. (2018). On the need for regional climate information over Africa under varying levels of global warming. *Environmental Research Letters*, 13(6), 060401.
- Li, J., Zhang, X. Y., & Yang, Y. Z. (2012). SWAT model of runoff study under different land use land cover scenarios in source region of the Yangtze River. *Research of Soil and Water Conservation*, 19(3), 119–124.
- Li, S., Jin, B., Wei, X., Jiang, Y., & Wang, J. (2015). Using CA-Markov model to model the spatiotemporal change of land use/cover in Fuxian Lake for decision support. International workshop on spatiotemporal computing, 13–15 July 2015, Fairfax, Virginia.
- Luo, K., Tao, F., Moiwo, J. P., & Xiao, D. (2016). Attribution of hydrological change in Heihe River basin to climate and land use change in the past three decades. *Scientific Reports*, 6, 33704.
- Mwangi, W. W., Ho, K. W., Tey, B. T., & Chan, E. S. (2016). Effects of environmental factors on the physical stability of pickering-emulsions stabilized by chitosan particles. *Food Hydrocolloids*, 60, 543–550.
- Natkhin, M., Dietrich, O., Schäfer, M. P., & Lischeid, G. (2015). The effects of climate and changing land use on the discharge regime of a small catchment in Tanzania. *Regional Environmental Change*, 15(7), 1269–1280.
- Negewo, T. U. F. A., & Sarma, A. K. (2021). *Evaluation of climate change-induced impact on streamflow and sediment yield of Genale watershed, Ethiopia*. IntechOpen. <https://doi.org/10.5772/intechopen.98515>

- Neitsch, S. L., Arnold, J. G., Kiniry, J. R., & Williams, J. R. (2011). Soil & Water Assessment Tool Theoretical Documentation Version 2009, Texas Water Resources Institute Technical Report No. 406, Texas A & M University System, Texas, USA, <https://hdl.handle.net/1969.1/128050>
- Ning, T., Li, Z., & Liu, W. (2016). Separating the impacts of climate change and land surface alteration on runoff reduction in the Jing River catchment of China. *Catena*, 147, 80–86.
- Pontius, G. R., & Malanson, J. (2005). Comparison of the structure and accuracy of two land change models. *International Journal of Geographical Information Science: IJGIS*, 19(2), 243–265.
- Rajib, A., & Merwade, V. (2017). Hydrologic response to future land use change in the Upper Mississippi River Basin by the end of 21st century. *Hydrological Processes*, 31(21), 3645–3661.
- Simane, B., Beyene, H., Deressa, W., Kumie, A., Berhane, K., & Samet, J. (2016). Review of Climate Change and Health in Ethiopia: Status and gap Analysis. *Ethiopian Journal of Health Development*, 30(1 Spec Iss), 28–41.
- Singh, J., Knapp, H. V., Arnold, J. G., & Demissie, M. (2005). Hydrological modeling of the Iroquois River watershed using HSPF and SWAT. *JAWRA Journal of the American Water Resources Association*, 41, 343–360.
- Stanzel, P., Kling, H., & Bauer, H. (2018). Climate change impact on West African rivers under an ensemble of CORDEX climate projections. *Climate Services*, 11, 36–48.
- Tesfaye, S., Taye, G., Birhane, E., & van der Zee, S. E. (2019). Observed and model simulated twenty-first century hydro-climatic change of northern Ethiopia. *Journal of Hydrology Regional Studies*, 22, 100595.
- Tessema, N., Kebede, A., & Yadeta, D. (2021). Modelling the effects of climate change on streamflow using climate and hydrological models: The case of the Kesem sub-basin of the Awash River basin, Ethiopia. *International Journal of River Basin Management*, 19, 469–480.
- Teutschbein, C., & Seibert, J. (2012). Bias correction of regional climate model simulations for hydrological climate-change impact studies: Review and evaluation of different methods. *Journal of Hydrology*, 456–457, 12–29.
- Trolle, D., Nielsen, A., Andersen, H. E., Thodsen, H., Olesen, J. E., Børgesen, C. D., Refsgaard, J. C., Sonnenborg, T. O., Karlsson, I. B., Christensen, J. P., Markager, S., & Jeppesen, E. (2019). Effects of changes in land use and climate on aquatic ecosystems: Coupling of models and decomposition of uncertainties. *The Science of the Total Environment*, 657, 627–633.
- Tumsa, B. C. (2022). Performance assessment of six bias correction methods using observed and RCM data at upper Awash basin, Oromia, Ethiopia. *Journal of Water and Climate Change*, 13(2), 664–683. <https://doi.org/10.2166/wcc.2021.181>
- Umair, M., Kim, D., & Choi, M. (2019). Impacts of land use/land cover on runoff and energy budgets in an East Asia ecosystem from remotely sensed data in a community land model. *The Science of the Total Environment*, 684, 641–656.
- Wang, H., Tetzlaff, D., & Soulsby, C. (2018). Modelling the effects of land cover and climate change on soil water partitioning in a boreal headwater catchment. *Journal of Hydrology*, 558, 520–531.
- Wedajo, G. K., Muleta, M. K., & Awoke, B. G. (2022). Impacts of combined and separate land cover and climate changes on hydrologic responses of Dhidhessa River basin, Ethiopia. *International Journal of River Basin Management*. 1–14. <https://doi.org/10.1080/15715124.2022.2101464>
- Worqlul, A., Dile, Y. T., Ayana, E., Jeong, J., Adem, A., & Gerik, T. (2018). Impact of climate change on streamflow hydrology in headwater catchments of the Upper Blue Nile Basin, Ethiopia. *Water*, 10, 120.
- Yang, L., Feng, Q., Yin, Z., Wen, X., Si, J., Li, C., & Deo, R. C. (2017). Identifying separate impacts of climate and land use/cover change on hydrological processes in upper stream of Heihe River, Northwest China. *Hydrological Processes*, 31(5), 1100–1112.
- Yesuph, A. Y., & Dagnaw, A. B. (2019). Land use/cover spatiotemporal dynamics, driving forces and implications at the Beshillo catchment of the Blue Nile Basin, North Eastern Highlands of Ethiopia. *Environmental Systems Research*, 8(1), 1–30.
- Yifru, B. A., Chung, I. M., Kim, M.-G., & Chang, S. W. (2021). Assessing the effect of land/use land cover and climate change on water yield and groundwater recharge in East African Rift Valley using integrated model. *Journal of Hydrology Regional Studies*, 37, 100926.
- Yin, J., He, F., Xiong, Y. J., & Qiu, G. Y. (2017). Effects of land use/land cover and climate changes on surface runoff in a semi-humid and semi-arid transition zone in northwest China. *Hydrology and Earth System Sciences*, 21(1), 183–196.
- Zhang, L., Karthikeyan, R., Bai, Z., & Srinivasan, R. (2017). Analysis of streamflow responses to climate variability and land use change in the Loess Plateau region of China. *CATENA*, 154, 1–11.
- Zuo, C., Huang, L., Zhang, M., Chen, Q., & Asundi, A. (2016). Temporal phase unwrapping algorithms for fringe projection profilometry: A comparative review. *Optics and Lasers in Engineering*, 85, 84–103.